The High-Resolution Architecture and Structural Dynamics of *Bacillus* Spores

Marco Plomp,* Terrance J. Leighton,† Katherine E. Wheeler,† and Alexander J. Malkin*
*BioSecurity and Nanosciences Laboratory, Lawrence Livermore National Laboratory, Livermore, California; and
†Children's Hospital Oakland Research Institute, Oakland, California

ABSTRACT The capability to image single microbial cell surfaces at nanometer scale under native conditions would profoundly impact mechanistic and structural studies of pathogenesis, immunobiology, environmental resistance, and biotransformation. Here, using in vitro atomic force microscopy, we have directly visualized high-resolution native structures of bacterial endospores, including the exosporium and spore coats of four *Bacillus* species in air and water environments. Our results demonstrate that the mechanisms of spore coat self-assembly are similar to those described for inorganic and macromolecular crystallization. The dimensions of individual *Bacillus atrophaeus* spores decrease reversibly by 12% in response to a change in the environment from fully hydrated to air-dried state, establishing that the dormant spore is a dynamic physical structure. The interspecies distributions of spore length and width were determined for four species of *Bacillus* spores in water and air environments. The dimensions of individual spores differ significantly depending upon species, growth regimes, and environmental conditions. These findings may be useful in the reconstruction of environmental and physiological conditions during spore formation and for modeling the inhalation and dispersal of spores. This study provides a direct insight into molecular architecture and structural variability of bacterial endospores as a function of spatial and developmental organizational scales.

INTRODUCTION

Bacterial endospores are models for elucidating mechanisms of dormancy, chemical cueing of germination and pathogenesis. Even though complete genome sequences are available for *Bacillus subtilis, Bacillus cereus, Bacillus thuringiensis,* and *Bacillus anthracis*, the relationships between spore architecture, spore coat topology and spore function are not understood. The spore coat (Driks, 2002) is a structural and reactive barrier that protects interior spore compartments including the DNA-containing core. In some spore-forming species, including *B. anthracis*, the etiological agent of anthrax, an exosporium structure overlays the spore coat. The role of these structures in determining spore hydrophobicity, adhesion, dispersal, and resistance to environment stresses is poorly understood.

Analysis of spore architecture (Aronson and Fitz-James, 1976; Wehrli et al., 1980) has relied on electron microscopy (EM) techniques that frequently require sample preparation methods such as fixation, staining, dehydration, and embedding that can damage the native structural integrity of biological specimens. An alternative high-resolution method to examine native spore ultrastructure is atomic force microscopy (AFM), which allows direct visualization of macromolecular assemblies at molecular resolution (Binnig et al., 1986; Bustamante et al., 1997; Muller and Engel, 1999; Kim et al., 2000; Shao et al., 2000; Stolz et al., 2000). We have recently demonstrated the ability of AFM to reveal native surface structures of several pathogens at ~20–30 Å resolution (Plomp et al., 2002; Malkin et al., 2003, 2004; Malkin and McPherson, 2004) under physiological conditions. The resolution of AFM was comparable to that of cryo-EM (Plomp et al., 2002; Malkin et al., 2004), and viruses of different, but closely related, families could be discriminated on the basis of structural variations (Malkin et al., 2004). We have also shown that viral internal structures could be exposed and analyzed with chemical and enzymatic nano-dissection (Plomp et al., 2002; Malkin et al., 2003).

AFM studies of fungal spores have revealed the presence of rodlet structures within the spore coat and allowed mapping of adhesion on the spore surface (Dufrêne et al., 1999). Recently, the surface morphology of bacterial spores was investigated by AFM (Chada et al., 2003); however, high-resolution structural analysis of bacterial spores has not been demonstrated with AFM methods.

In this study we have utilized in vitro AFM to visualize high-resolution native structures of bacterial endospores including the exosporium and crystalline layers of the spore coat of several *Bacillus* species in fully hydrated and air-dried states. Variations in spore coat architecture appear to be a consequence of species-specific crystallization mechanisms that regulate the assembly of the outer spore coat. Direct visualization of the environmental response of individual *Bacillus atrophaeus* spores revealed that upon air-drying, spore dimensions decreased by ~12%, followed by a nearly complete recovery in size upon rehydration. The observed decrease in the size of bacterial spores and concomitant change in spore coat surface morphology after

Submitted July 9, 2004, and accepted for publication October 13, 2004.

Address reprint requests to Alexander J. Malkin, Tel.: 925-423-7817; Fax: 925-422-2041; E-mail: malkin1@llnl.gov.

0006-3495/05/01/603/06 $2.00

doi: 10.1529/biophysj.104.049312

dehydration are due to the contraction of the internal spore core and/or cortex. We also determined the intra- and interspecies distributions of spore length and width for four species of *Bacillus* spores in fully hydrated and air-dried states. It was found that the dimensions of individual spores differ significantly depending upon species, growth regimes, and environmental conditions.

MATERIALS AND METHODS

Spore preparation and purification

Spore preparations were produced using Schaeffer's sporulation medium as previously described (Longchamp and Leighton, 2000). Solid phase spore preparations were produced on agar plates containing Schaeffer's sporulation medium solidified with 1.5% DIFCO agar (BD Diagnostic Systems, Sparks, MD). Spores were purified as previously described (Nicholson and Setlow, 1990). *B. atrophaeus* (ATCC 9372) and *Bacillus thuringiensis israelensis* (ATCC 35646) were obtained from the American Type Culture Collection (ATCC; Manassas, VA). The *B. subtilis* 168 strain has been described previously (Longchamp and Leighton, 2000). Sonication was performed using a 20-kHz 130-W Vibra-cell VC 130 (Sonics and Materials, Newtown, CT) with a 3-mm probe. Spores were sonicated in an Eppendorf tube for 5 s, interspersed with 20-s cooling intervals (4°C) to prevent excessive heating of the sample. The amplitude was increased from 0% to 30% and decreased to 0% for moderate sonication treatments, and increased to 50% for more intense sonication treatments (*B. cereus* spores). Spores were treated for 10–20 cycles of sonication.

Atomic force microscopy

For AFM observation, droplets of spore suspensions were deposited on mica, HOPG graphite, or plastic cover slips and incubated for 10 min, after which the sample substrate was carefully rinsed. For experiments in liquid, the resulting sample was imaged using an AFM fluid cell. For experiments in air, the sample was dried and imaged.

We used Digital Imaging (DI, Santa Barbara, CA) Nanoscope IIIa and IV atomic force microscopes operated in tapping mode. The AFM instruments were equipped with optical microscopes, which enabled us to track individual spores for imaging after a change of the environment. Before the change in the environment, large scan areas (~40 μm) were visualized with AFM, and digital photographs of the surrounding area (~2 mm) were taken using the optical microscope. We utilized fiducial points (marks on the substrate, large conglomerates of spores) for repositioning of the AFM probe and tracking previously imaged individual spores after the environmental change.

For imaging in air, DI and Olympus etched silicon tips with force constants of ~40 N/m and resonance frequencies of ~300 kHz were used. For imaging in water, DI and Olympus silicon nitride cantilevers (force constant 0.1 N/m) with either etched silicon or oxide-sharpened silicon nitride tips were used. Tapping amplitude, phase and height images were collected simultaneously. Height images were primarily used for quantitative measurements and amplitude and phase images were predominantly used for presentation.

For spore size determination, we measured both spore height and length. We assume height, just as spore width measured elsewhere using EM (Leuschner et al., 1999) and optical microscopy (Westphal et al., 2003), to be identical to the semiminor axis (Westphal et al., 2003) and length to be identical to the semimajor axis (Westphal et al., 2003). Throughout the text we refer to height measurements as width measurements.

Dull or contaminated AFM tips can produce artifactual images of spores and other biological samples (Malkin et al., 2004). Due to the limited sharpness of the AFM tip (Velegol et al., 2003), artifacts can also arise when imaging relatively large particles such as spores. Size measurements in the lateral AFM image plane can also have systematic errors, which differ from tip to tip. Therefore, each series of size measurements was performed with one single tip to avoid systematic errors within a series. AFM height measurements do not suffer from this problem, and hence are more reproducible irrespective of tip geometry. Height measurements were used exclusively for monitoring the dynamics of individual spore size responses to changes from water to air environments.

RESULTS AND DISCUSSION

Spore topography

To study the topology and architecture of the outer spore integuments we visualized liquid and air-dried spore preparations from *B. thuringiensis, B. cereus, B. subtilis,* and *B. atrophaeus* (Fig. 1, *a*, *d*, and *g*). *B. thuringiensis* and *B. cereus* spores are enclosed in an exosporium (Fig. 1, *a* and *d*), which is considerably larger than the underlying spore. The high-resolution structure of the exosporium of *B. cereus* spores (*inset*, Fig. 1 *b*) is composed of 12–14 nm diameter subunits, which could represent exosporial proteins or their oligomers.

Removal of the *B. thuringiensis* (Fig. 1 *a*) and *B. cereus* (Fig. 1 *d*) exosporium by sonication revealed crystalline hexagonal honeycomb (Fig. 1 *c*) and rodlet (Fig. 1 *e*) outer spore coat structures, respectively. The ~10-nm thick rodlet layer of *B. cereus* spores is formed by multiple randomly oriented domains, comprised of parallel subunits with a periodicity of ~8 nm. The size of the domains is typically 100–200 nm. Complete removal of the exterior *B. cereus* rodlet layer by sonication revealed an underlying honeycomb structure (Fig. 1 *f*) similar to the exterior spore coat layer of *B. thuringiensis* (Fig. 1 *c*). For both species, the lattice parameter for the honeycomb structure is ~9 nm, with ~5–6-nm holes/pits (Fig. 1, *c* and *f*).

For *B. atrophaeus* (Fig. 1 *g*) and *B. subtilis* spores (data not shown here), the outer spore coat was composed of a crystalline rodlet layer with a periodicity of ~8 nm (Fig. 1 *h*). In contrast to the multidomain rodlet structure of the *B. cereus* spore coat (Fig. 1 *e*), generally only a single continuous domain was found to be present on the outer coat of *B. atrophaeus* and *B. subtilis* spores.

Similar rodlet and honeycomb crystalline structures to those seen in Fig. 1 were observed in freeze-etching EM studies of several species of *Bacillus* spores (Aronson and Fitz-James, 1976; Wehrli et al., 1980) and AFM studies of fungal spores (Dufrêne et al., 1999). In the case of *B. thuringiensis*, spore coat rodlet structures were not observed in freeze-etching EM (Aronson and Fitz-James, 1976; Wehrli et al., 1980) or in the current AFM studies. However, as illustrated in Fig. 1 *i*, patches of adsorbed rodlets were observed on the substrate during AFM visualization of *B. thuringiensis* spores. Rodlet width and thickness (Fig. 1 *e*) were similar to those observed for *B. atrophaeus* and *B. cereus* spore coat structures (Fig. 1, *e* and *h*), which indicates that similar rodlet proteins could be present during

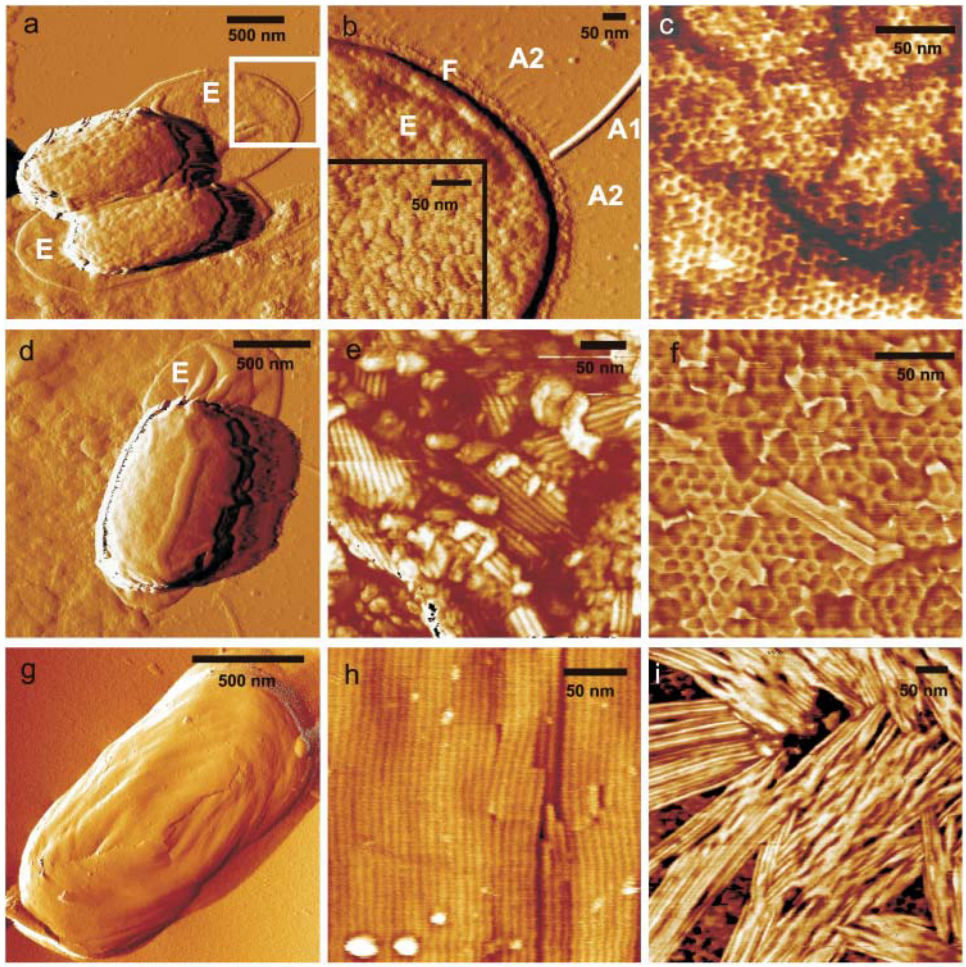

FIGURE 1 The spore coats of *B. thuringiensis* (*a–c*), *B. cereus* (*d–f*), and *B. atrophaeus* (*g* and *h*) consist of crystalline layers of honeycomb and rodlet structures. *B. thuringiensis* (*a*) and *B. cereus* (*d*) spores are surrounded by an exosporium (*E*), which collapses and adheres to the substrate when spores are air-dried. The exosporium (*b*) is 25–40-nm thick and has a ~3-nm thick and 20–30-nm wide footstep (*F*) with numerous thin (~1 nm) and short (50–60 nm) hair-like appendages (*A2*) attached to it. Additionally, there are typically 4–8 tubular appendages (*A1*) attached to the exosporium with diameters and lengths of 3–12 nm and 300–1200 nm, respectively. Underneath the exosporium, a honeycomb crystalline layer defines the outer surface of *B. thuringiensis* spores (*c*). This honeycomb layer is formed by domains with random crystalline orientations that are separated by linear defects. In *e* and *h*, the crystalline rodlet structures of *B. cereus* and *B. atrophaeus* spore coats are shown. *B. cereus* spores contain a crystalline honeycomb structure (*f*) beneath the exterior rodlet layer. *B. thuringiensis* spore coats do not contain rodlet structures. Rodlet assemblies can be seen adsorbed to the substrate (*i*). Scale bar, 500 nm in *a*, *d*, and *g*; 50 nm in *b*, *c*, *e*, *f*, *h*, and *i*.

sporulation in these three species of *Bacillus* spores. However, rodlets do not nucleate and grow on the outer coat of *B. thuringiensis* spores. Under different physiological conditions, it is possible that rodlets could assemble on the *B. thuringiensis* spore surface.

The striking differences in native rodlet motifs seen in *B. atrophaeus* (one major domain for each spore), *B. cereus* (a patchy multidomain motif), and *B. thuringiensis* (extrasporal rodlets) appear to be a consequence of species-specific nucleation and crystallization mechanisms which regulate the assembly of the outer spore coat. The control of rodlet crystallization could depend on morphogenetic assembly factors, composition and concentration of the growth units, as well as on environmental factors, such as temperature, pH, metals, and salts. In the case of *B. cereus* outer coat assembly, the surface free energy (Chernov, 1984) for crystalline phase nucleation appears to be low enough to allow the formation of multiple rodlet domains resulting in cross-patched and layered assemblies. During the assembly of the outer coat of *B. atrophaeus* spores, the surface free energy may be considerably higher; reducing nucleation to the point that only one major domain is formed covering the entire spore surface.

All *Bacillus* species investigated utilize very similar rodlet structures as spore coat building blocks. The mechanisms of self-assembly of spore coat structural layers appear to be closely related to those described for crystallization of inorganic single crystals (Chernov, 1984) and macromolecular crystals grown for x-ray diffraction analysis (McPherson, 1999; Vekilov and Chernov, 2002). Consequently, fundamental and applied concepts developed for the growth of inorganic and protein crystals can be successfully applied to study the assembly of the spore coat. The solution chemistry (i.e., concentration of assembly factors, spore coat proteins, small molecules, pH, temperature, etc.) during spore integument formation may control the macromolecular arrangement of rodlet motifs. Indeed, it has been reported that the addition of Na_2SO_3 during sporulation of *B. cereus* caused rodlet elongation and incomplete rodlet layer assembly (Aronson and Fitz-James, 1976). These observations suggest that spore coat architecture and topology are genetically and

environmentally determined, and that AFM analysis could be used to reconstruct the environmental conditions that were present during spore formation.

Spore response to a change in the environment from fully hydrated to air-dried state

Detailed knowledge of the physical response of spores to changes in their environment is paramount for understanding their structural dynamics, germination, and inactivation by decontamination regimes. AFM allows a side-by-side comparison of high-resolution structures, morphology and individual spore dimensions in fully hydrated (Fig. 2 *a*) and air-dried states (Fig. 2 *b*). An air to water phase transition does not affect the microscopic arrangement of the *B. atrophaeus* rodlet structure. However, upon drying, a significant deformation of the entire spore coat was observed (Fig. 2 *b*), resulting in the generation of 30–60-nm thick ridges extending along the entire spore surface with a number of shorter 5–15-nm thick wrinkles. Upon rehydration, a smooth and continuous rodlet layer, similar to one seen in Fig. 2 *a*, was reestablished (data not shown). Dehydration induced surface ridges (Fig. 2 *b*) have been observed previously in EM (Holt and Leadbetter, 1969) and AFM (Chada et al., 2003) studies of bacterial spores.

Formation of ridges upon dehydration was found to be accompanied by a pronounced decrease in spore size. The average width of 35 individual spores in air (65% relative humidity) was reduced to 88% of the size measured for aqueous phase spores (Fig. 2 *c*). When the dried spores were rehydrated, they returned to 97% of their original size after 2 h in water, establishing the reversibility of the size transition. These individual spore measurements were confirmed by independent studies where *B. atrophaeus* spore width was measured from two independent sets of ~200 spores in water and air, respectively. The air-dried spore width was again reduced by 12% when compared to spores imaged in water. The observed decrease in the width of bacterial spores upon dehydration is apparently due to contraction of the spore core and/or cortex.

The size dynamics reported here confirm and extend recent experiments of two of the authors (Westphal et al., 2003), where, using optical microscopy, a reversible size change of ~4% was measured for *B. thuringiensis* spores upon a change of relative humidity from 3% to >95%. Based on these experiments, it was further suggested (Driks, 2003) that the morphology of the spore coat could change upon swelling or shrinking of the spore. The direct visualization of individual spore environmental responses to dehydration/rehydration presented here clearly demonstrates that the spore coat itself does not shrink/expand but is flexible enough to compensate for the internal volume decrease of core/cortex compartments by surface folding and formation of ridges.

These studies establish that the dormant spore is a dynamic physical structure. Spore swelling could play an important role during emergence from the dormant state. Preliminary AFM studies suggest that additional alterations of spore dimensions accompany the initial stages of the germination process.

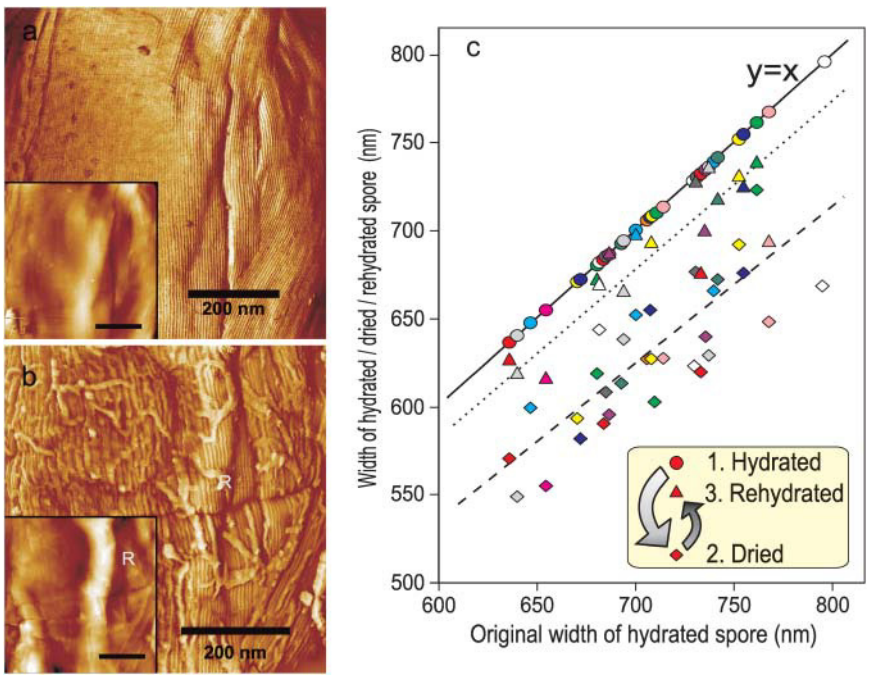

FIGURE 2 The effects of changing the *B. atrophaeus* spore environment from hydrated to dehydrated states. (*a*) Phase image and height image (*inset*) detail of a *B. atrophaeus* spore in water, showing several shallow wrinkles. (*b*) The same spore after drying, showing many adsorbed stray rodlets, and a 60-nm high ridge (indicated with *R*). Loose stray rodlets sediment from the bulk solution upon drying of the sample. Stray rodlets are present on the surfaces of all air-dried spores. (*c*) Width change of 35 individual *B. atrophaeus* spores. Depicted is the individual measured spore width for a set of dehydrated (24 h) (*diamonds, dashed trend line*) and rehydrated (2 h) spores (*triangles*, *dotted trend line*), as a function of the size of the originally hydrated spore. For ease of comparison, the original hydrated spore width is (redundantly) depicted as circles, which by definition lie on the solid $y = x$ line. Thus, the three data points for one individual spore, depicted with the same color, are all on the same vertical line. Several spores detached from the substrate during rehydration, which resulted in fewer experimental points for rehydrated spores (*triangles*). On average, spore size is reduced to 88% for dried spores, and returns to 97% of the original width for rehydrated spores (see text). Scale bar in *a* and *b*, 200 nm.

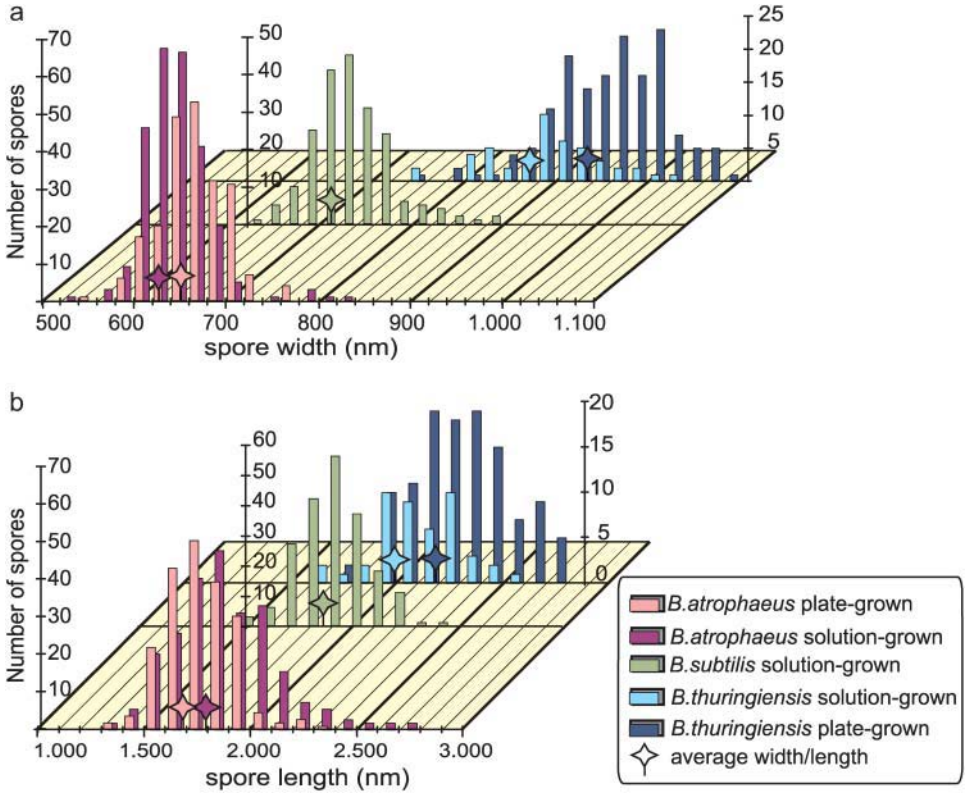

FIGURE 3 Distribution of spore width (*a*) and length (*b*) for plate-grown (*pg*) and solution-grown (*sg*) *B. atrophaeus* and *B. thuringiensis* spores, and solution-grown *B. subtilis* spores. Average width and length are indicated with stars. Statistics for these distributions are given in Table 1.

Spore size distribution

Size distributions from several large (~200) populations of spores were determined. Both spore width and length were measured for hydrated and dried solution- and plate-grown *B. atrophaeus*, dried solution- and plate-grown *B. thuringiensis* and dried and solution-grown *B. subtilis* spores, respectively (Fig. 3). The average values for spore width W_{av} and length L_{av} are given in Table 1, together with the absolute deviation D, defined as:

$$D_{x\ (x=W,L)} = \frac{1}{N}\sum_{i=1}^{N}|x_i - x_{av}|. \quad (1)$$

From these measurements, the deviation in width is 4–6% and for length is 7–13%.

By comparison, using EM images, the standard deviation for length and width of various *B. subtilis* spores was measured to be ~12% (Leuschner et al., 1999). In our studies, the EM measurements are approximately comparable to a standard deviation of 5–8% (length) and 8–17% (width). The difference between the smallest and largest spores observed was a factor of ~1.5× in width, and approaches a factor of 2× for length. Even in the case of a single spore-forming species and controlled growth conditions, there is a wide distribution of smaller and larger size spores that could have significantly different dispersal, deposition, and inhalation characteristics. The observed spore dimension variations within a single population are of particular importance to models that predict the environmental fate, transport, and settling velocity of spores.

Spores of *B. thuringiensis* are substantially larger (~50% higher and ~20% longer) than *B. atrophaeus* and *B. subtilis* spores. The difference in average width and length between plate-grown and solution-grown spores of *B. atrophaeus* and *B. thuringiensis* suggest that environmental/physiological factors can have significant effects on spore dimensions.

TABLE 1 Average width, length, and absolute deviations for several spore populations

	No. spores	W_{av} (nm)	D_W (nm)	D_W (%)	L_{av} (μm)	D_L (μm)	D_L (%)
B. atrophaeus sg dried	264	626	27	4.2%	1.79	0.19	10%
B. atrophaeus pg dried	220	647	28	4.3%	1.68	0.13	7.8%
B. subtilis sg dried	202	713	32	4.5%	1.85	0.12	6.6%
B. thuringiensis sg dried	46	872	47	5.4%	2.00	0.16	7.8%
B. thuringiensis pg dried	153	937	49	5.3%	2.17	0.18	8.3%

sg, solution-grown; pg, plate-grown; W_{av}, L_{av}, average width and length; D_W, D_L, absolute deviation in width and length.

We have demonstrated that AFM can address spatially explicit spore coat protein interactions and their structural consequences at near-molecular resolution. For the first time, *Bacillus* species-specific spore coat crystalline layers were observed at high-resolution in their natural environment, namely air and water. We have also utilized AFM for high-resolution measurements of individual bacterial spore dynamics and intra- and interspecies size distribution analyses. These studies establish AFM as a powerful new tool capable of revealing bacterial spore structure and variability at nanometer-to-micrometer scales.

We thank A. McPherson for the use of the scanning probe microscope facilities in his laboratory at the University of California, Irvine; S. Velsko and J. J. DeYoreo for helpful discussions and encouragement; and M. Pitesky for providing samples for initial experiments.

This work was performed under the auspices of the U.S. Department of Energy by the University of California, Lawrence Livermore National Laboratory, under Contract W-7405-Eng-48 and with support from the Defense Advanced Research Projects Agency.

REFERENCES

Aronson, A. I., and P. Fitz-James. 1976. Structure and morphogenesis of the bacterial spore coat. *Bacteriol. Rev.* 40:360–402.

Binnig, G., C. F. Quate, and C. Gerber. 1986. Atomic force microscope. *Phys. Rev. Lett.* 56:930–933.

Bustamante, C., C. Rivetti, and D. Keller. 1997. Scanning force microscopy under aqueous solutions. *Curr. Opin. Struct. Biol.* 7:709–716.

Chada, V. G. R., E. A. Sanstad, R. Wang, and A. Driks. 2003. Morphogenesis of *Bacillus* spore surfaces. *J. Bacteriol.* 185:6255–6261.

Chernov, A. A. 1984. Modern Crystallography III. Crystal Growth. Springer-Verlag, Berlin.

Driks, A. 2002. Maximum shields: the assembly and function of the bacterial spore coat. *Trends Microbiol.* 10:251–254.

Driks, A. 2003. The dynamic spore. *Proc. Natl. Acad. Sci. USA.* 100:3007–3009.

Dufrêne, Y. F., C. J. P. Boonaert, P. A. Gerin, M. Asther, and P. G. Rouxhet. 1999. Direct probing of the surface ultrastructure and molecular interactions of dormant and germinating spores of *Phanerochaete chrysosporium*. *J. Bacteriol.* 181:5350–5354.

Holt, S. C., and E. R. Leadbetter. 1969. Comparative ultrastructure of selected aerobic spore-forming bacteria: a freeze etching study. *Bacteriol. Rev.* 33:346–378.

Kim, H., R. M. Garavito, and R. Lal. 2000. Atomic force microscopy of the three-dimensional crystal of membrane protein, OmpC porin. *Coll. Surf. B: Biointerfaces.* 19:347–355.

Leuschner G. K., A. C. Weaver, and P. J. Lillford. 1999. Rapid particle size distribution analysis of *Bacillus* suspensions. *Coll. and Surf. B.* 13: 47–57.

Longchamp, P., and T. Leighton. 2000. Molecular recognition specificity of *Bacillus globigii* spore antibodies. *Lett. Appl. Microbiol.* 31:242–246.

Malkin, A. J., and A. McPherson. 2004. Probing of crystal interfaces and the structures and dynamic properties of large macromolecular ensembles with in situ atomic force microscopy. *In* From Solid-Liquid Interface to Nanostructure Engineering, Vol. 2: Assembly in Hybrid and Biological Systems. X. Y. Lin, and J. J. DeYoreo, editors. Plenum/Kluwer Academic Publisher, New York. 201–238.

Malkin, A. J., A. McPherson, and P. D. Gershon. 2003. Structure of intracellular mature vaccinia virus visualized by *in situ* AFM. *J. Virol.* 77:6332–6340.

Malkin, A. J., M. Plomp, and A. McPherson. 2004. Unravelling of the architecture of human viruses by high-resolution atomic force microscopy. *In* Methods in Molecular Biology: DNA Viruses: Methods and Protocols. P. M. Lieberman, editor. Humana Press, Totowa, NJ. 85–108.

McPherson, A. 1999. Crystallization of Biological Macromolecules. Cold Spring Harbor Laboratory Press, Cold Spring Harbor, NY.

Muller, D., and A. Engel. 1999. Voltage and pH-induced channel closure of porin OmpF visualized by atomic force microscopy. *J. Mol. Biol.* 285:1347–1351.

Nicholson, W. L., and P. Setlow. 1990. Sporulation, germination, and outgrowth. *In* Molecular Biological Methods for Bacillus. C. R. Harwood and S. M. Cutting, editors. John Wiley & Sons, Chichester, UK. 391–450.

Plomp, M., M. K. Rice, E. K. Wagner, A. McPherson, and A. J. Malkin. 2002. Rapid visualization at high resolution of pathogens by atomic force microscopy: structural studies of herpes simplex virus-1. *Am. J. Pathol.* 160:1959–1966.

Shao, Z., D. Shi, and A. V. Somlyo. 2000. Cryoatomic force microscopy of filamentous actin. *Biophys. J.* 78:950–958.

Stolz, M., D. Stoffler, U. Aebi, and C. Goldsbury. 2000. Monitoring biomolecular interactions by time-lapse atomic force microscopy. *J. Struct. Biol.* 131:171–180.

Vekilov, P. G., and A. A. Chernov. 2002. The physics of protein crystallization. *In* Solid State Physics, Vol. 5. H. Ehrenreich and F. Spaepen, editors. Academic Press, New York. 1–147.

Velegol, S. B., S. Pardi, X. Li, D. Velegol, and B. E. Logan. 2003. AFM imaging artifacts due to bacterial cell height and AFM tip geometry. *Langmuir.* 19: 851–857.

Wehrli, E., P. Scherrer, and O. Kubler. 1980. The crystalline layer in spores of *Bacillus cereus* and *Bacillus thuringiensis* studied by freeze-etching and high resolution electron microscopy. *Eur. J. Cell. Biol.* 20:283–289.

Westphal, A. J., P. Buford Price, T. J. Leighton, and K. E. Wheeler. 2003. Kinetics of size changes of individual *Bacillus thuringiensis* spores in response to changes in relative humidity. *Proc. Natl. Acad. Sci. USA.* 100:3461–3466.